INELASTIC PROCESSES IN 0.1-1000 keV/u COLLISIONS OF Ne^{q+} (q=7-10) IONS WITH ATOMIC HYDROGEN

D.R. Schultz and P.S. Krstić
Controlled Fusion Atomic Data Center
Oak Ridge National Laboratory
Oak Ridge, Tennessee 37831-6373, USA

Abstract: Owing to the potential use of neon as an intentionally introduced radiating impurity in fusion reactor divertors, we present here cross sections for (*i*) ionization, (*ii*) state-selective excitation, and (*iii*) state-selective charge transfer in 0.1-1000 keV/u collisions of Ne^{q+} (q=7-10) with H. The cross sections may be used in modeling and diagnosing the distribution and state of these ions as well as other parameters of the core, edge, and divertor regions of the plasma. We have utilized the theory of hidden crossings in the low energy portion of the energy range considered and the classical trajectory Monte Carlo method throughout the high energy portion.

1. INTRODUCTION

The previous decades have shown an ever closer approach to the goal of break-even in fusion reactors. As this goal is obtained, the direction of research will turn more and more towards the physics and engineering study of burning plasmas. Therefore, with the production of significant quantities of fusion-product helium, and significant fusion energy, it is necessary to consider how to exhaust this helium ash, how to recycle hydrogen, and how to remove heat from the plasma. Cooling is required both to extract heat to run turbines producing electricity (obviously the ultimate practical goal of fusion research) and to prevent the temperature of the plasma facing components from reaching too high a temperature.

Thus, much effort is being devoted to devising, engineering, and modeling reactor divertors through which these goals may be achieved, particularly for experimental devices already in existence (e.g. JET) and for the proposed *International Thermonuclear Experimental Reactor*. One of the primary difficulties has been that the early schemes for such a divertor would have potentially subjected the divertor plates to a very large amount of energy (e.g. 20 to 40 MW/m^2 or more [1]). In contrast, current designs call for the reduction of this tremendous heat and particle flux by using atomic processes in a rather open region, often referred to as a "gaseous divertor" and by spreading the load over a much larger surface area than originally envisioned. In particular, charge transfer, hydrogen and impurity radiation, ionization, and elastic collisions between the recycling gas and the divertor plasma are predicted to disperse the heat [2, 3].

In addition, it is estimated that the radiation from hydrogen will not be sufficient and some impurity species will have to be introduced into the divertor region to increase the radiation losses. Since these losses increase with increasing nuclear charge, Z, and since any large contamination of the core plasma by high-Z impurities will quench the plasma, a delicate balance in the choice of what species to introduce must be made. It is predicted that impurities introduced by puffing into the edge or divertor become entrained to some extent, and that this will therefore limit the potential deleterious radiation losses.

One suitable impurity for this task seems to be neon. Its nuclear charge is high enough to induce a significantly increased amount of radiation in the divertor, potentially without reaching a fatal fraction in the core. In addition, since neon would not ordinarily be present in a reactor as would species composing the plasma facing walls (Ni, Fe, Be, C, etc.) or occuluded gases (e.g. oxygen), neon would be a good diagnostic species. If detected, it could have only originated from the point of injection, and only in the amount injected. Thus techniques such as charge exchange recombination spectroscopy could be used to track the motion of the neon ions and their spatial and charge state distributions to determine the parameters of the plasma such as temperature, density, and rotation.

Therefore, in order to provide a preliminary database for modeling and diagnosis that incorporates the inelastic collisions involving neon ions and atomic hydrogen, we present here the (*i*) ionization, (*ii*) state-selective excitation, and (*iii*) state-selective charge transfer cross sections in 0.1-1000 keV/u collisions of Ne^{q+} (q=7-10) with H. We apply two methods which have been shown to provide reliable results over complementary energy ranges, the theory of hidden crossings (HC), and the classical trajectory Monte Carlo (CTMC) technique. Since each of these methods treats an ion-atom collision as possessing transitions of only a single electron, we cover a range of ionic charge states of neon for which we can be assured that there is little effect of electrons contained by the projectile exchanging with that of the target, or being ionized or excited. Further, we apply the models only to those charge states where the computed charge transfer cross section is not appreciably affected by capture to unphysical states. That is, for the partially stripped ions, if the model results in capture to principal quantum levels that are in actuality filled, then a clear signal that a more robust model must be employed is present.

In the following sections we quite briefly summarize the CTMC and HC methods and then present and tabulate our results for the inelastic cross sections.

2. THEORY

A large body of work has shown that the CTMC method provides a reasonable and accurate estimate of these cross sections for intermediate collision velocities for bare ions colliding with H, H_2, and He. Some results have also been obtained for partially stripped impinging ions with reasonable agreement found with experiments, but with less overall certainty, since a full treatment would have to include the multielectronic transitions possible in such a case. Since theoretical methods with which a large range of ionic charges and collision energies could be covered more robustly is not readily available, the CTMC results provide a first estimate of the required processes.

That is, the complete quantum mechanical treatment of an arbitrary ion, carrying possibly several electrons, colliding with atomic or molecular hydrogen, is a difficult, multi-electron, many-state calculation. The CTMC technique, in its one-active-electron, many-active-electron, or model-potential formulations serves as a very useful tool to produce a broad range of required data. Careful comparison with other more robust methods for a set of fundamental channels allows one to assess the range of reliability of the CTMC results, and to extend with some reasonable level of confidence to other similar systems. Previous works have, for example, tabulated state selective charge transfer cross sections for C^{6+} and O^{8+} with atomic hydrogen [4] and He^{2+} with H in both the ground and n=2 states of hydrogen [5], and total electron loss cross sections for Fe ions colliding with H, H_2, and He [5].

The basic CTMC method has been described by Abrines and Percival [6] and Olson and Salop [7], and particular applications pertinent to computing excitation by Reinhold, Olson, and Fritsch [8], state-selective capture by Becker and MacKellar [9] (see also Refs. [4, 5]), and for collisions in which the inactive projectile electrons are represented by a model potential by Peach *et al.* [10] and Toburen *et al.* [11], for example. An independent work, using a slightly different form of the model potential has also been performed using CTMC for charge transfer and ionization in Ne^{q+} + H by Maynard *et al.* [12]. The present results generally agree with these, but are extended here to describe excitation of the target, and to tabulate the charge transfer cross sections to the n, ℓ levels.

The cross sections have been computed concerning ionization and charge transfer for neon ions colliding with atomic hydrogen using CTMC, and matched in the region of energy around the maximum of the cross section with results of the theory of hidden crossings.

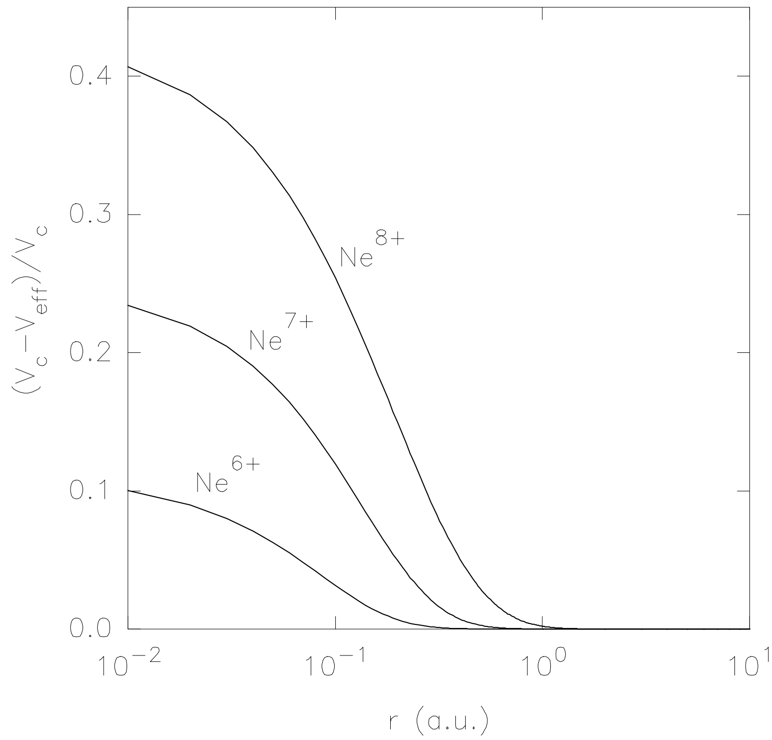

Figure 1: *The relative deviation of the independent particle model potential [20] for* Ne^{q+} *(q=6,7,8) from the Coulomb potential of a bare ion of charge* $q+1$ *versus electron distance from the nucleus.*

The advanced adiabatic method, also known as the hidden crossing method, utilizes the strong localization of the nonadiabatic transitions at low collision energies between two quasimolecular states to those internuclear distances where respective quasimolecular electronic eigenenergies cross [13]. Since, according to Wigner-Neumann noncrossing rule, the states of the same symmetry (that radially couple) cannot cross for real R, the localization of the strong transitions is shifted to the plane of complex internuclear distances R, where the adiabatic electronic Hamiltonian is no longer Hermitian. When R is extended formally to the plane of complex R, the eigenvalues and eigenfunctions of the instantaneous electronic adiabatic Hamiltonian H(R) of a two-center–one-electron system are analytic functions. This is a consequence of the analyticity of H(R). The only singularities have the nature of branch points that connect pairwise different branches of the single, multivalued eigenenergy function E(R). If R is real, these branches coincide with the electronic eigenenergies.

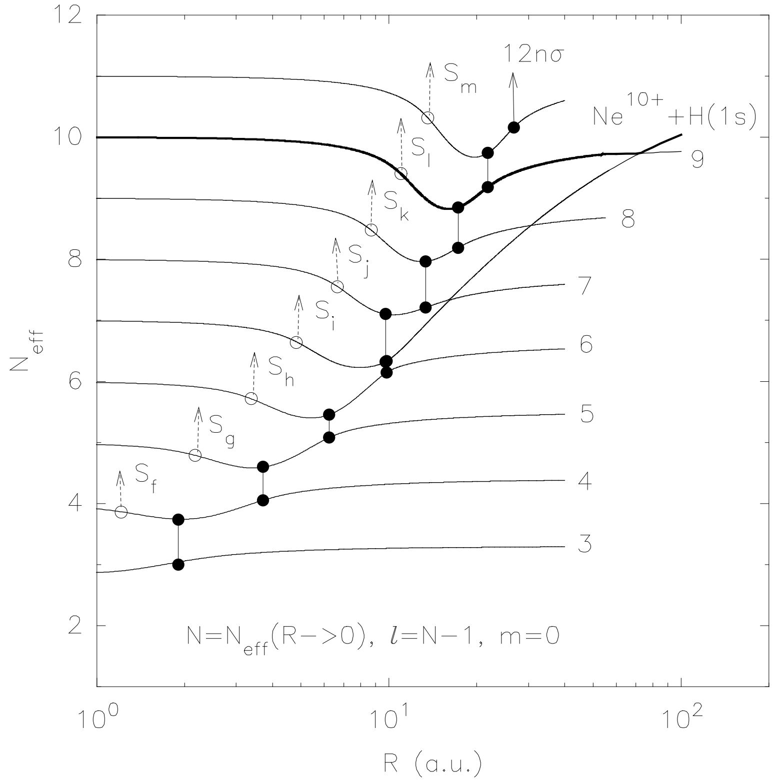

Figure 2: *Quasimolecular, adiabatic electronic energies for the σ states for the Ne^{10+} + H collision system expressed in terms of the effective principal quantum number in the united atom limit, $N_{eff} = 11/\sqrt{-2E_{N\ell\sigma}}$. Only those ionic curves of $Ne^{9+}(n) + H^{+}$that are coupled radially with the initial state, $Ne^{10+} + H(1s)$,via the Q type transitions (filled circles), are shown. (Hollow circles, localization of the S superseries; "crossings" of the curves are the isolated Landau-Zener avoided crossings [15], which do not belong to the Q superseries).*

The branch points (hidden crossings) define the localization of the radial nonadiabatic transitions. Circulation around a branch point R_b promotes one branch E_α of the Riemann surface E(R) to another one, E_β, thus making a transition between two quasimolecular states, α and β . The probability of the transition is given by a simple exponential form,

$$P_{\alpha\beta} = \exp(-2\frac{\Delta_{\alpha\beta}}{v}) \tag{1}$$

where v is the collision velocity and

$$\Delta_{\alpha\beta} = \left| Im \int_{\alpha\beta} \frac{E_{\alpha\beta}}{v_R/v} dR \right| \tag{2}$$

is the generalized Massey parameter. The integral in Eq.(2) is taken along a contour around the point R_b, starting from real R at an energy E_α and ending at real R, at E_β. Finally, v_R is the radial velocity of the nuclear motion.

Thus, following in succession the pairwise transitions in the complex R plane, while the system evolves along the real R axis, one can obtain the probability of transition from an arbitrary initial to an arbitrary final state. These are the basic ideas of the hidden crossing theory [14, 15, 16, 17], which has been shown to be successful [18, 19] in calculation of total and partial cross sections for ionization, charge transfer, and excitation of one electron atoms in slow collisions with multicharged ions. The theory is exact in the low velocity limit, and its applicability extends to approximately the maximum of the cross section. The latter depends upon the system and the inelastic process in question.

Two principal kinds of branch points, those of the so-called S and Q types, have been defined according to different radial selection rules [15]. These were found to form superseries. The S superseries are localized in a narrow domain of the complex R plane, at small Re{R}, and constitute the transitions which pairwise, and in succession, connect the states (N, ℓ, m), $(N+1, \ell, m)$, $(N+2, \ell, m)$,... ((N, ℓ, m) are the spherical united atom quantum numbers). This localized set of transitions constitutes a strong mechanism which almost diabatically promotes the state $(N, N-1, m)$ into the continuum during the incoming phase of the collision. These superseries have a limiting point when $n \to \infty$, and are associated with passing the centrifugal barrier. The Q transitions are the main mechanism for charge transfer and excitation, and these connect (N, ℓ, m) and $(N+1, \ell+1, m)$ states. They also constitute superseries which in succession can promote a state to the continuum in the receding phase of the collision. The Q branch points are associated with passing the top of the Coulomb barrier and are found at larger internuclear distances.

The hidden crossing theory was originally developed for systems of the form (Z_2, e, Z_1). In principle, the method can be generalized to systems containing more than one electron, but this has not yet been accomplished in a reliable way. Nevertheless, it can be applied in its original formulation to the collisions of multielectron ions with one-electron atoms if the effective potential of the ion is Coulombic for those internuclear distances where the transitions are localized. In Figure 1 we show the relative deviation of the effective multielectron potential from the Coulomb potential, $(V_c - V_{eff})/V_c$, for the ions $Ne^{q+}, q = 6, 7, 8$, where V_{eff} is defined as the effective one-electron potential of the multielectron atom given by Szydlik and Green [20]. A similar potential is used in our CTMC calculations to model the Ne^{q+} ion. From the figure it is obvious that the electron moves in an almost pure Coulomb potential if its distance from the nucleus is larger than about one atomic unit.

This can be applied to the collision of these neon ions with hydrogen, whose electron can be captured by the ion already at larger internuclear seperation. When the internuclear distance R>1, the overlap of the active electron wavefunction in the initial hydrogenic and final ionic state is that of Coulombic functions. Figure 2 shows the electronic energy diagram of the $(NeH)^{10+}$ system, for the manifold of σ states. The adiabatic energy curve of the initial $Ne^{10+} + H(1s)$ state is shown by the thick solid line. The Q transitions and the S superseries are denoted by the filled and hollow circles, respectively. Besides these, three isolated Landau-Zener type avoided crossings appear. These diabatically promote the initial state of the system to $7i\sigma$ adiabatic state, and charge transfer and ionization are consequences of the subsequent coupling of this state with others, via the Q and S type branch points. The populations of the states far from the $7i\sigma$ state decreases rapidly. On the other hand, the positions of the important S and Q transitions (other than for very low lying states, which are only populated weakly) is of the order of R=10. These branch points are shifted toward smaller values, as the charge of the ion decreases. Nevertheless, if the collision of Ne^{7+} with H is modeled by the $N^{7+} + H$ system, on the basis of Figure 1 (with q=6), the relevant S and Q transitions stay well beyond R=1. This justifies the application of the two-center–one-electron hidden crossing theory to collisions of hydrogen with Ne^{q+} ions with $q = 7, 8, 9, 10$.

Besides the S and Q type transitions, and their relevant superseries, we also calculate transitions induced by rotation of the internuclear axis at small internuclear distances. These transitions couple states of different magnetic quantum number m, within a fixed ℓ and N. Inclusion of the rotational coupling shifted the charge transfer cross section maxima toward smaller energies, and significantly increased the cross sections at the lowest energies.

The total number of the branch points used in the calculations of ionization and charge transfer were as follows: 1) 68 for the $(NeH)^{10+}$ system; 2) 82 for $(NeH)^{9+}$ (modeled by the $(FH)^{9+}$ system); 3) 75 for $(NeH)^{8+}$ ($(OH)^{8+}$), and 4) 72 for $(NeH)^{7+}$ ($(NH)^{7+}$).

3. IONIZATION

In Figure 3 we compare the present CTMC and HC results for the ionization of atomic hydrogen by Ne^{7-10+} ions over the collision energy range of 1 to 1000 keV/u. It has generally been found that below the maximum of the cross section the hidden crossings technique accurately predicts the cross section, while from just below this point to just past the maximum, the CTMC model is within its established limits of applicability. Thus, a smooth curve joining the CTMC and HC results, extending from low to intermediate energies provides a reasonable recommended cross section. For these collision systems, it appears that CTMC is valid down to 10 to 20 keV/u and up to at least 1 MeV/u (higher energies are not of present interest for fusion research). Similarly, we would recommend the HC result up to about 50 keV/u, with perhaps an averaging of HC and CTMC in the region in which these ranges overlap. The change in slope of the CTMC cross sections near 10 keV/u is most likely real, and we ascribe it to an effect described by Fritsch [21] as a type of orbital resonance, and also shown in both atomic orbital and CTMC calculations for beryllium ions colliding with atomic hydrogen [22].

We note that our CTMC results generally agree with those of Maynard *et al.* [12], but differ slightly, most likely owing to the use of a somewhat different model potential to represent the inactive electrons on the projectile. For the fully stripped ion, where this difference could not account for the discrepancies, there appears to be rather good agreement. The primary differences show up in the detailed shape of the cross sections. For example, from the figures in Ref. [12], it appears that the ordering of the ionization cross section at, say, 1000 keV/u are in order of increasing ionic charge state. That is, at this energy Ne^{10+} has the largest ionization cross section, followed by the 9+, 8+, and 7+ ions in that order. We however find an ordering of 9+, 10+, 8+, 7+. Since the cross sections are all within less than fifty percent of one another throughout much of the entire energy range considered here, small variations of the shape of

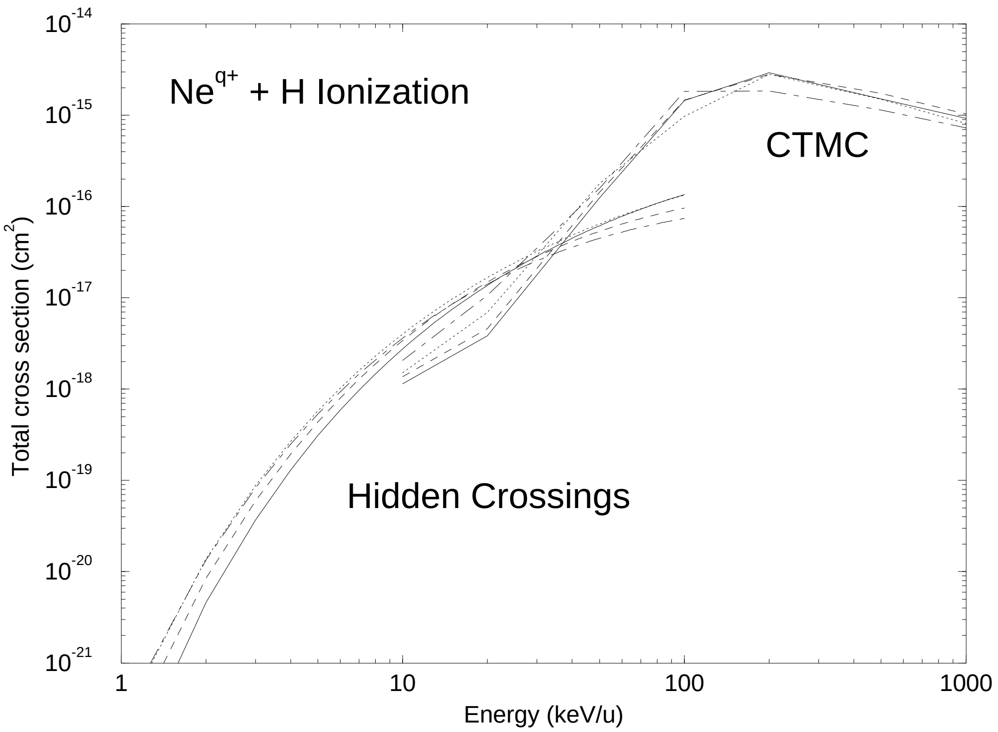

Figure 3: *The total cross section for ionization of H(1s) in collisions with* Ne^{q+} *(q=7-10) in the CTMC and HC models. (Solid curves,* Ne^{10+}*; dashed curves,* Ne^{9+}*; dotted curves,* Ne^{8+}*; dot-dashed curves,* Ne^{7+}*).*

the model potential could easily account for this differences.

Certain trends in the variations of the ordering of the cross sections according to charge are quite real. For example, at high energies, the highest charge states should indeed produce the greatest amount of ionization. However, this effect is not as large as one would expect on the basis of first order perturbation theory, and the assumption of a fully stripped projectile. In that case, the cross section would scale as the charge state squared (i.e. as q^2). It should be noted that as the charge state is increased, the q^2 scaling is known to break down even for fully stripped projectiles, and the cross section saturates. For Ne^{7-9+}, the projectile is only partially stripped, but, since in relatively small impact parameter collisions the target electron can experience the full nuclear charge, Z =10, the cross section for all of these ions peak at essentially the same value, reflecting this core penetration (for a more detailed discussion see e.g. [5]). In addition, at low energies, another effect leads to an inversion of the order of dominance of the charge states. In this case, since the higher charge state ions generally lead to a greater probability for charge transfer than do the ions of lower charge state, more flux is taken up by that channel, and the high-q ions have a lower ionization cross section.

4. EXCITATION

In Figures 4-7 we display the cross section for excitation of the initial ground state of atomic hydrogen to various final n-levels for the charge states 7+, 8+, 9+, and 10+, respectively. We

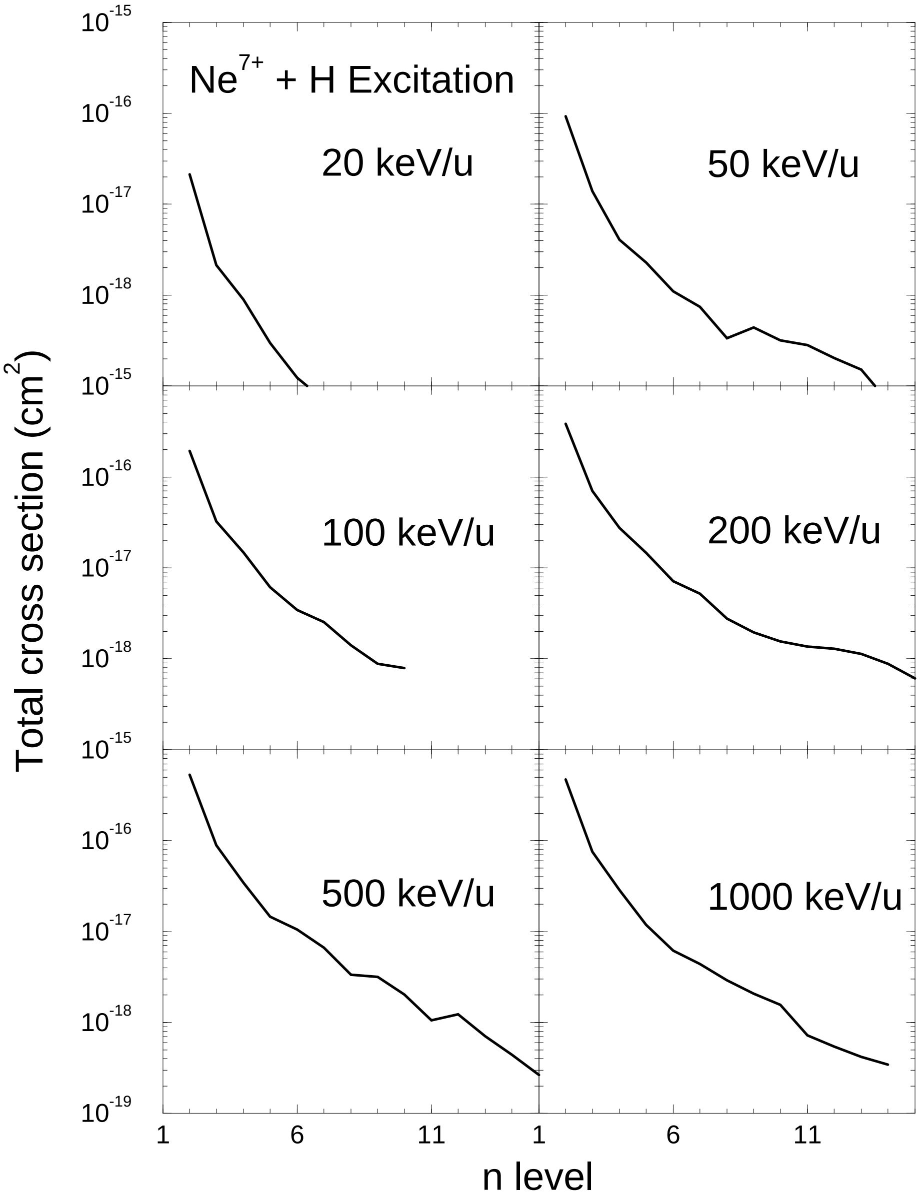

Figure 4: *The total cross section for excitation of H as a function of final n-level for several impact energies of Ne^{7+} computed using the CTMC method.*

note that the small fluctuations in the otherwise smooth dependence on n of these cross sections arises from the statistical uncertainty in the Monte Carlo sampling in the CTMC procedure, rather than from some physically significant process. In particular, for the largest cross sections, this uncertainty is very small (on the order of less than five percent) but for the smallest cross sections, it can be much larger.

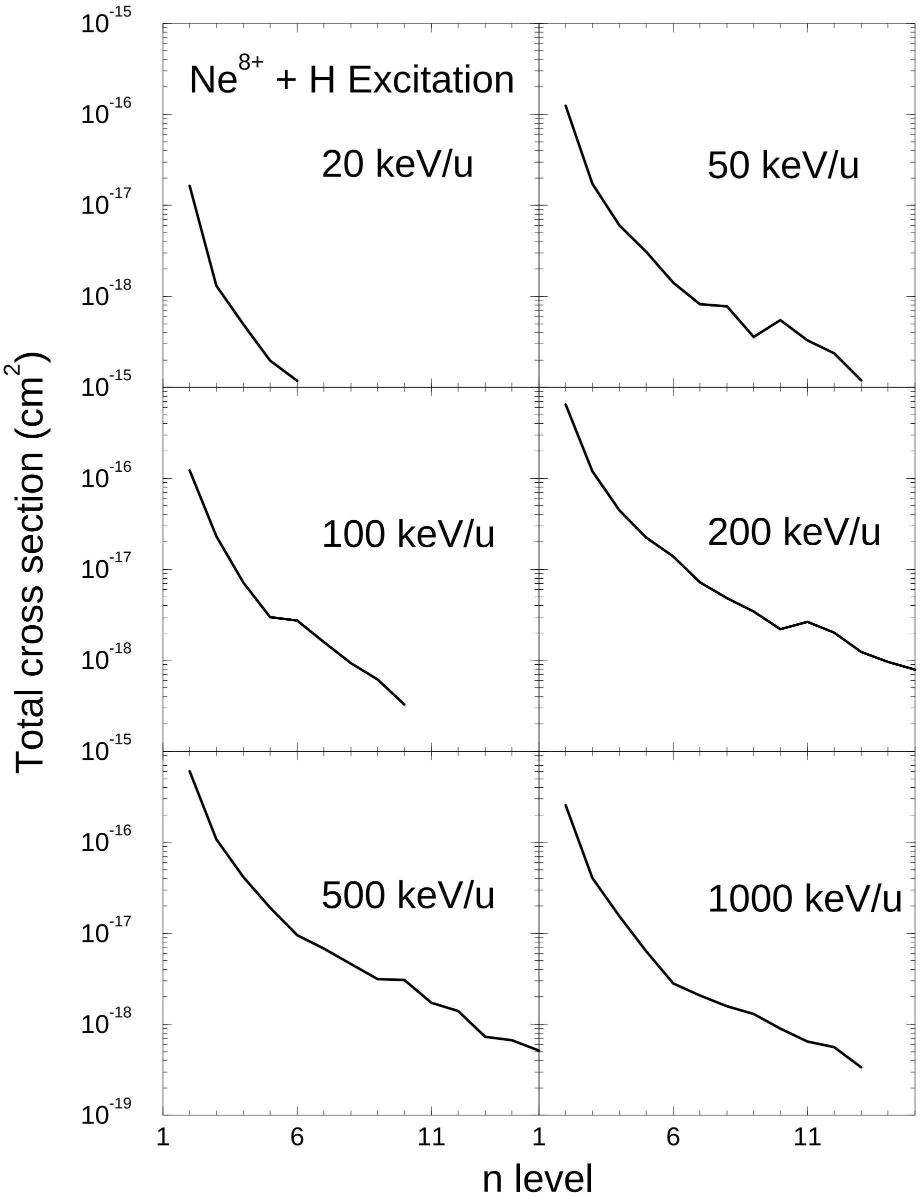

Figure 5: *The same as Figure 4 except for Ne^{8+}.*

Fitting a smooth curve through the points displayed readily demonstrates that above n=4, the well known scaling of the cross section as $1/n^3$ is obtained. Thus, these results give a point of reference for the low n-levels while results for the higher n-levels may be obtained from this scaling. Also readily seen from the figures is the fact that above about 20 keV/u, the distribution of n-levels populated, and the magnitude of the n-level cross sections does depend much on the ionic charge state of the neon ion, or the impact energy in the range 50 to 1000

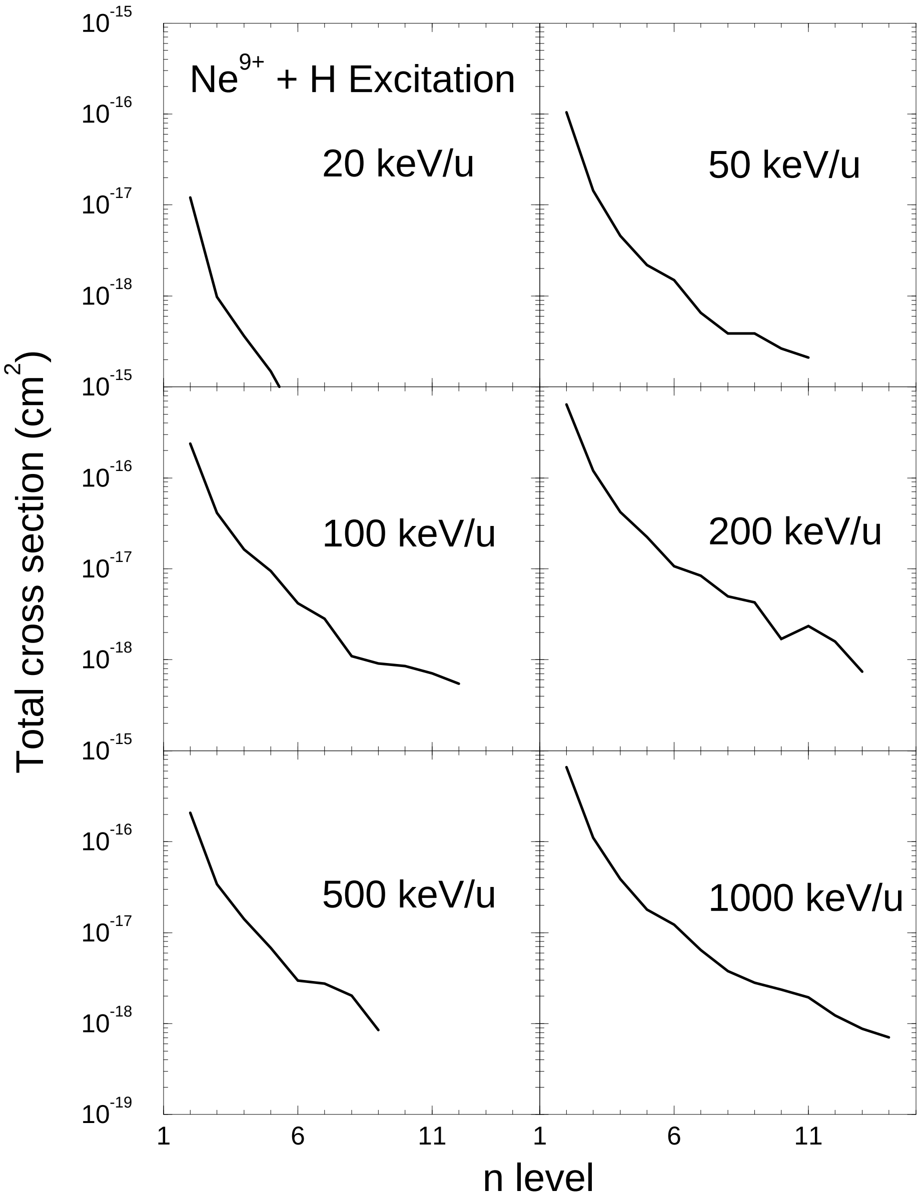

Figure 6: *The same as Figure 4 except for* Ne^{9+}.

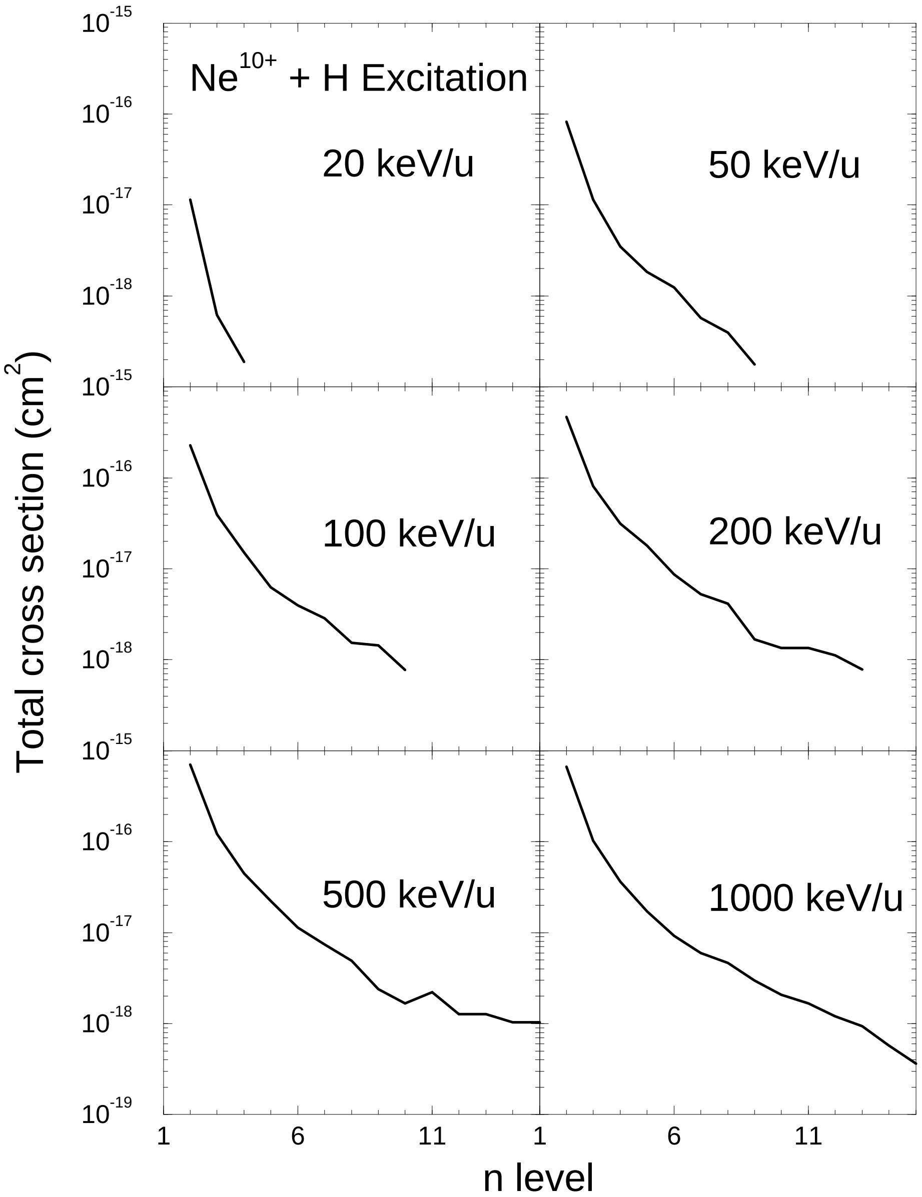

Figure 7: *The same as Figure 4 except for Ne^{10+}.*

keV/u. Similar to the situation obtained in ionization, collisions which penetrate the electronic core of the ion experience very similar charges close to the full nuclear charge, explaining the only slow variation of the magnitude of the cross section with changing ionic charge.

5. CHARGE TRANSFER

In Figure 8 we compare the results of the present HC and CTMC calculations regarding total charge transfer. In the energy range of approximately 1 to 100 keV/u, very good overal agreement exists between the two models. Below this energy, HC is expected to yield the appropriate behavior, while CTMC plateaus at low energy due to the fact that it essentially gives an over-the-barrier like result for capture into non-quantized energy levels. Above 100 keV/u the drop off of the cross section described by CTMC is expected to be the correct dependence of the process. As described in detail by Maynard *et al.* [12] a scaling of the cross section with impact energy and ionic charge state, q, may readily be deduced, and we refer the interested reader to their work.

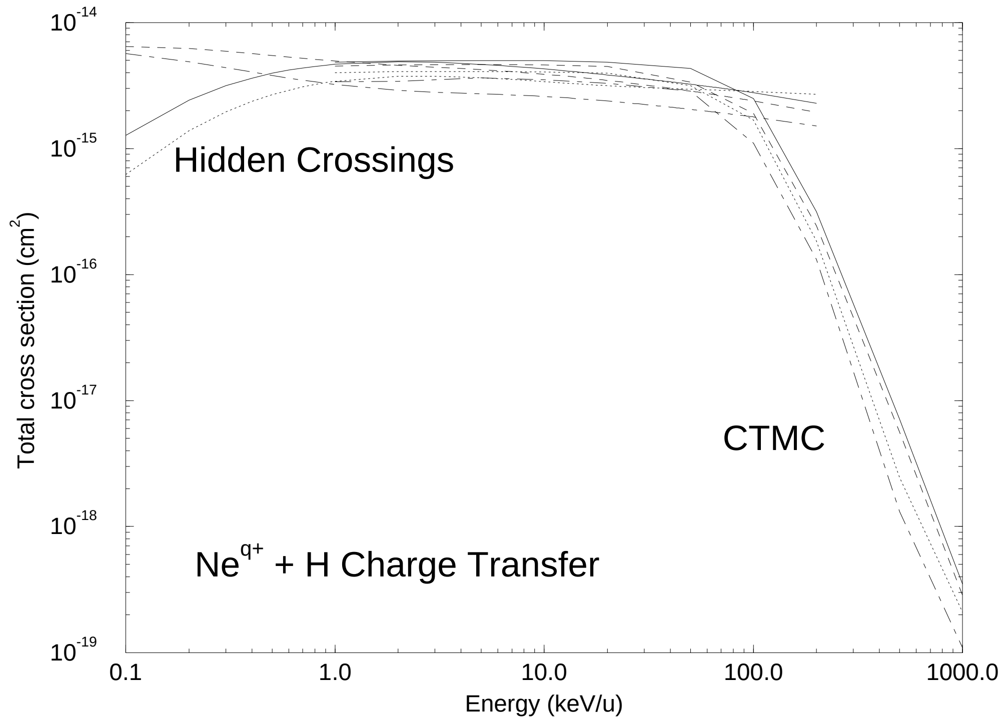

Figure 8: *Comparison of the HC and CTMC results for charge transfer in collisions of Ne^{q+} (q=7-10) with hydrogen. (Solid curves, Ne^{10+}; dashed curves, Ne^{9+}; dotted curves, Ne^{8+}; dot-dashed curves, Ne^{7+}).*

A more detailed comparison of the results of the two theories is presented in Figure 9. One sees that above 1 keV/u both methods agree on the ordering of the cross sections with ionic charge state. Below this energy, the quantum mechanical theory predicts that the cross section for the odd charge states should actually increase in magnitude, while the result for the even charge states decrease.

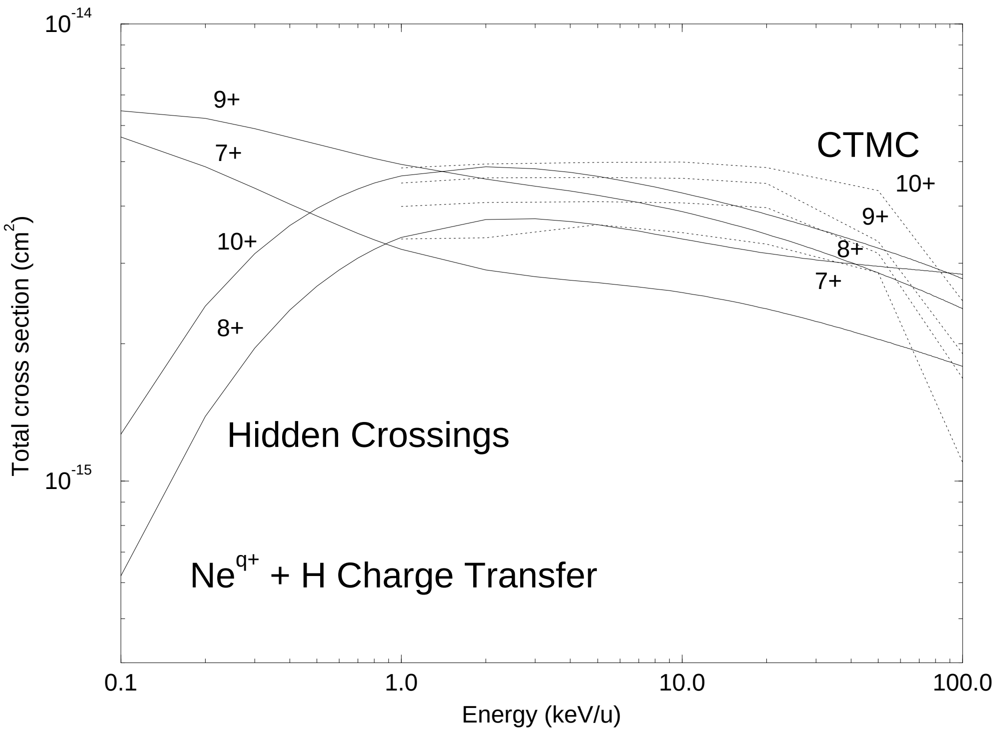

Figure 9: *A detailed comparison of the HC and CTMC results for charge transfer in collisions of* Ne^{q+} *(q=7-10) with hydrogen. Here the solid curves indicate the HC results and the dotted curves indicated the CTMC results. Neon ion charge states are indicated by the labels.*

Other features of the charge transfer process are illuminated by plotting the distribution of final n-level after capture, and also provide important practical information for plasma diagnostics and modeling. For example, in Figure 10 we display the n-level distribution for a wide range of impact energies for Ne^{7+} + H. Two characteristics are immediately observed. First, the distribution is most narrowly peaked in n for the lowest energies, becoming successively more broad as impact energy is increased. For the lowest energies, the distribution is nearly a delta function about the most likely n-level. Secondly, this value of n which is most likely to be populated in the charge transfer is given to good approximation by $n_{max} = q^{3/4}$. Such a propensity has been noted and explained previously (see Ref. [4] and references therein). The HC and CTMC models agree fairly well on the position of this maximum, but for this ion, the peaks are displaced by about one n-level. The agreement of the two theories is also very good regarding the magnitude of the cross section resolved at the n-level. By about 100 keV/u, the HC model begins to more seriously overestimate the magnitude at the peak, and fails to reflect the expected width of the distribution. Below 10 keV/u, the lack of quantized energy levels in CTMC seriously limits its applicability.

Figure 11 displays the same quantities as in Figure 10, but for Ne^{9+}. For the highest charge states of the ions, such as 9+ and 10+, HC and CTMC are found to compare very favorably. The shift of the predicted n_{max} noted for Ne^{7+} is not present, and again the magnitudes predicted are in excellent agreement up to about 50 keV/u.

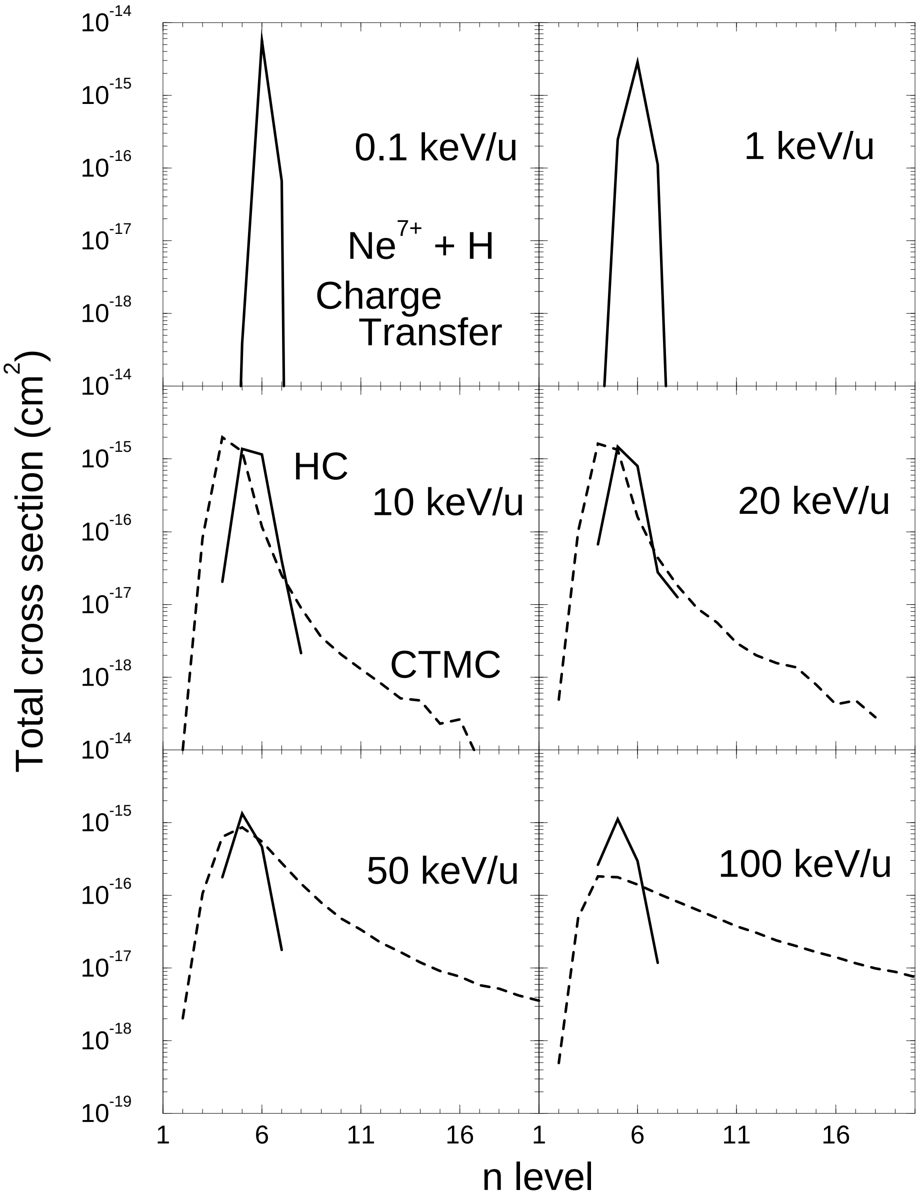

Figure 10: *The final n-level distribution after charge transfer in collisions of Ne^{7+} with hydrogen at several impact energy. The solid curves indicate the HC results and the dotted curves indicate the CTMC results.*

The energy dependence of the the n-resolved charge transfer cross sections is displayed in Figures 12-15 for Ne^{7-10+}. For the dominant capture channels (i.e. about n=4-6 or 7), HC and CTMC agree well at the point at which they intersect. However, for the non-dominant channels, the disagreement is significant. Therefore, we tabulate below the charge transfer cross section resolved by n and ℓ only for the groups of dominant channels where we can be assured that at least the n-resolved HC and CTMC results are in reasonable agreement. Thus, in Tables 1-4 we present n, ℓ charge transfer cross sections for Ne^{7-10+} + H for the dominant n-levels for 10, 20, 50, 100, and 200 keV/u computed using the CTMC method.

The ℓ distributions also reflect a particular behavior previously noted (see e.g. Ref. [4] and references therein). That is, for $n < n_{max}$, the ℓ distribution peaks more strongly to large ℓ

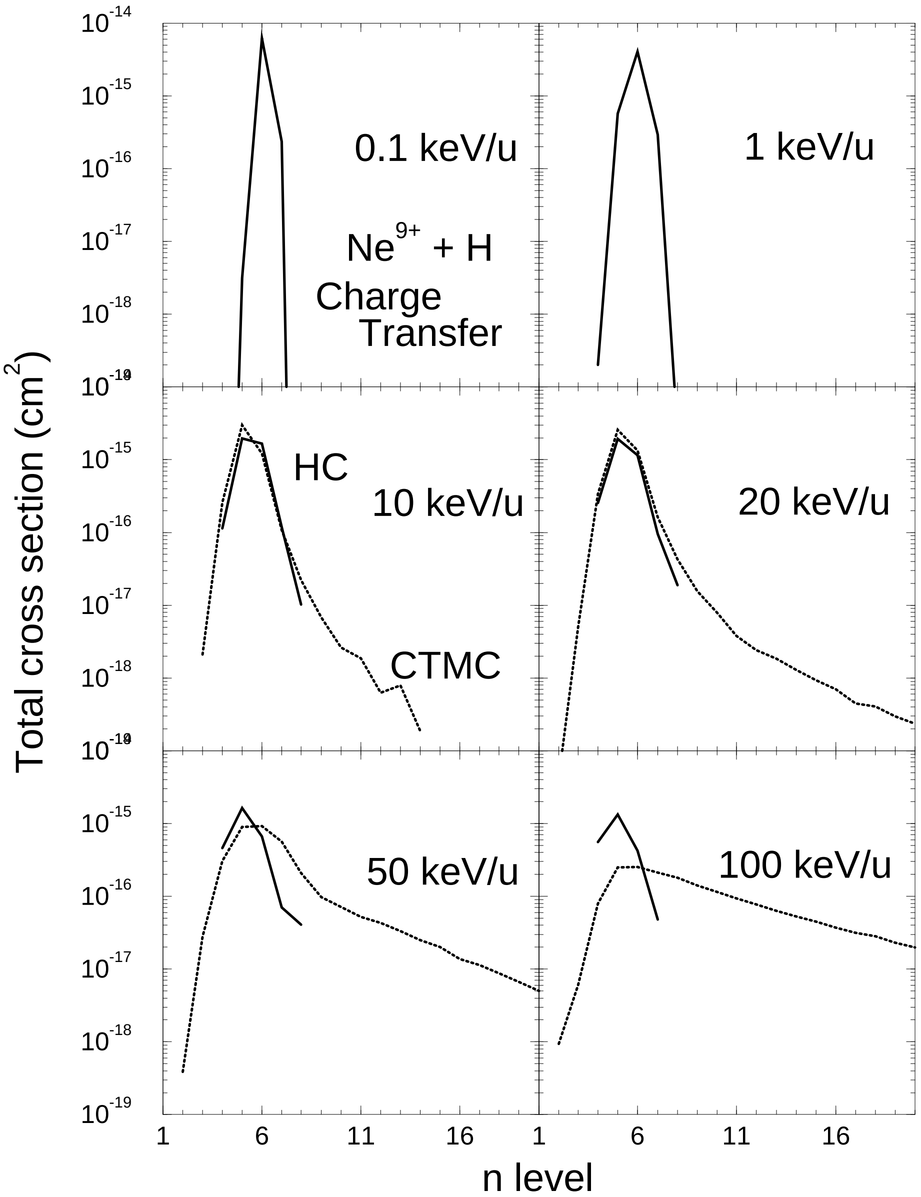

Figure 11: *The same as Figure 10 except for Ne^{9+}.*

than statistical, while for $n > n_{max}$, the distributions maximizes around $\ell = q^{3/4}$. These trends can more readily be observed from the distributions when not limited to the dominant channel results tabulated here.

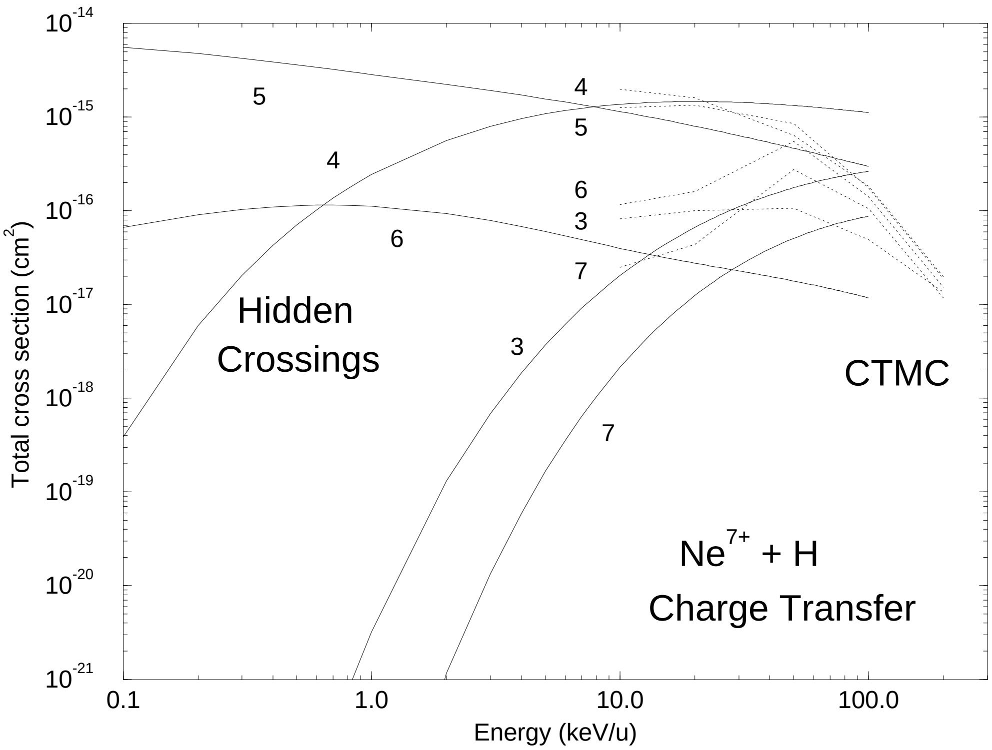

Figure 12: *Comparison of the CTMC and HC results for the energy dependence of the n-level cross section in charge transfer for $Ne^{7+} + H$. The solid curves indicate the HC results and the dotted curves indicate the CTMC results. The various n-levels are indicated by the labels.*

6. SUMMARY

Since the injection of neon into present and next-step fusion devices for diagnostic and plasma cooling purposes is of considerable current interest, we have presented an extensive comparison of results for ionization and state-selective charge transfer between a theory valid at low collision energies (the theory of hidden crossings) and another valid at higher energies (the classical trajectory Monte Carlo technique). We have displayed graphically the ionization, state-selective excitation, and state-selective charge transfer cross sections for Ne^{q+} (q=7-10) colliding with atomic hydrogen in the energy range 0.1 to 1000 keV/u. The present study has been limited to ions for which we can demonstrate a good likelihood that these one-active electron models will yield reasonable results. Finally, owing to the usefulness of the charge transfer cross section resolved by n and ℓ, we have tabulated these cross sections between 10 and 200 keV/u for the dominant n-levels.

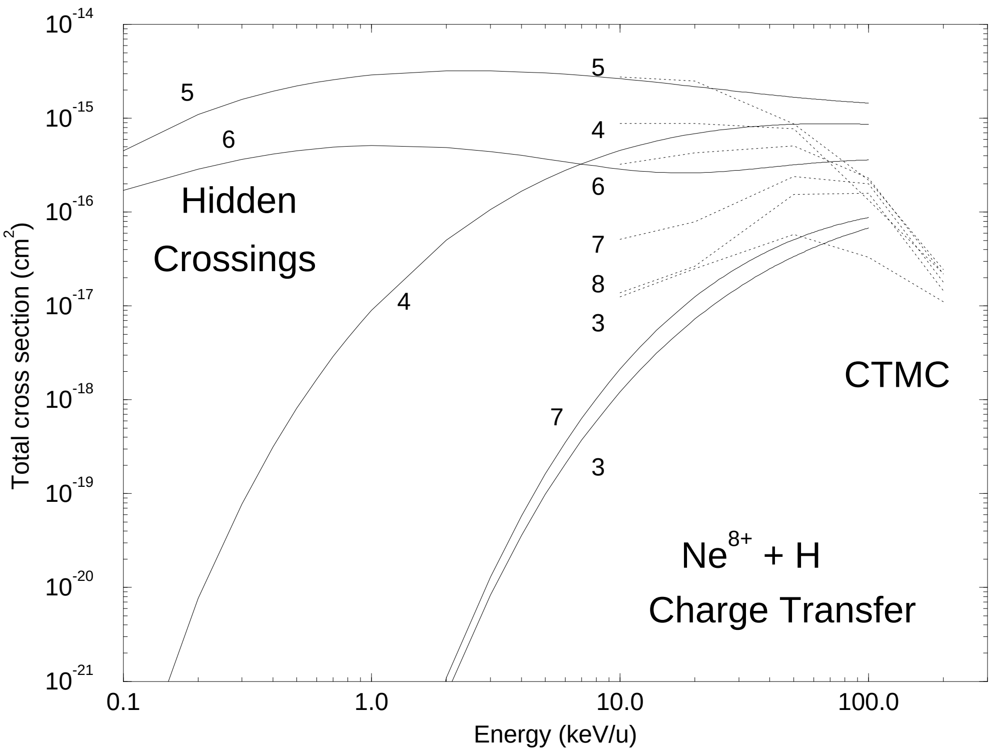

Figure 13: *The same as Figure 12 except for Ne^{8+}.*

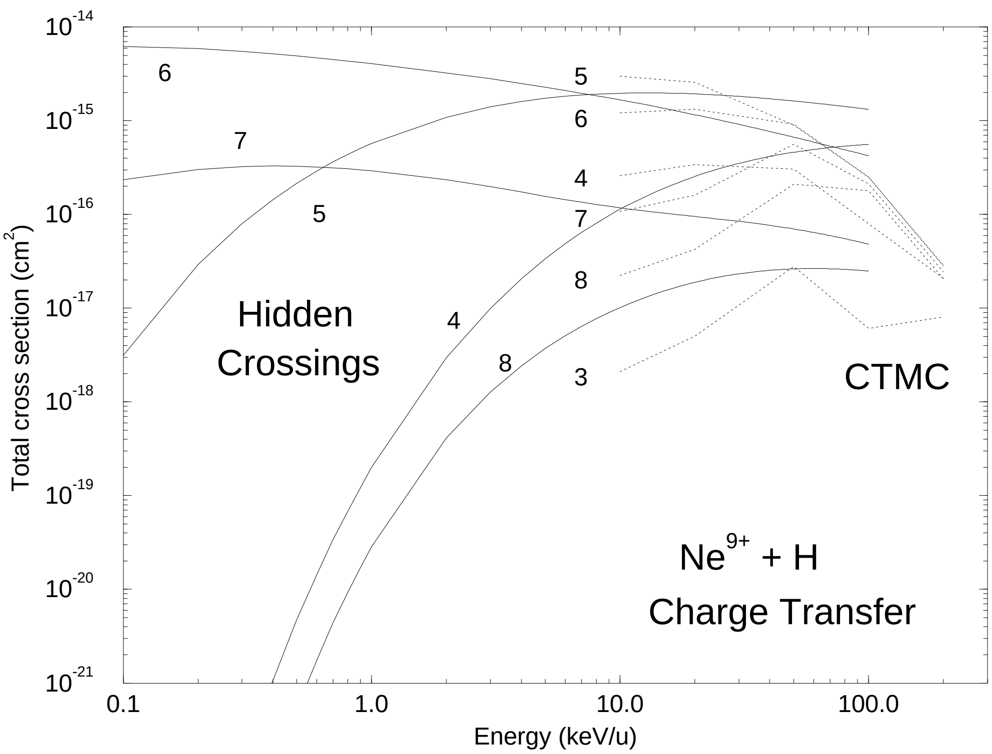

Figure 14: *The same as Figure 12 except for Ne^{9+}.*

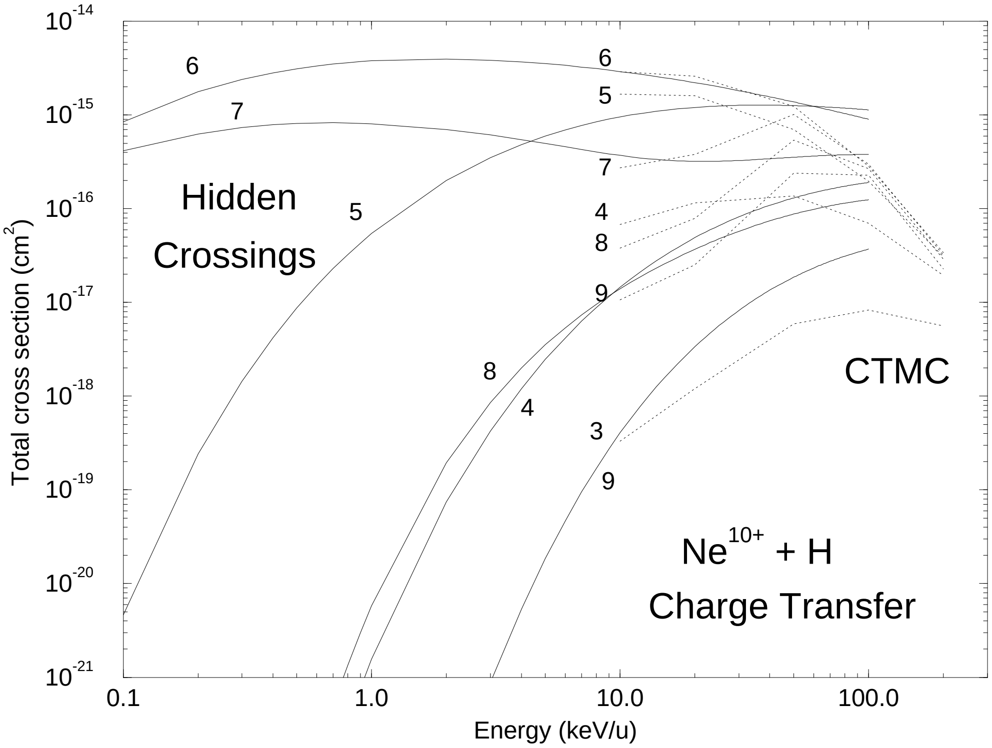

Figure 15: *The same as Figure 12 except for* Ne^{10+}.

Table 1: CTMC cross sections for charge transfer in 10, 20, 50, 100, and 200 keV/u Ne^{7+} + H. The table includes the n, ℓ-distribution for n=4, 5, and 6. Cross sections are given in cm^2.

10 keV/u				20 keV/u			
ℓ	n=4	n=5	n=6	ℓ	n=4	n=5	n=6
0	1.61E-16	2.98E-17	6.84E-18	0	6.02E-17	1.03E-17	3.32E-18
1	3.19E-16	6.53E-17	1.30E-17	1	1.81E-16	3.31E-17	9.75E-18
2	3.88E-16	1.15E-16	1.57E-17	2	3.94E-16	8.59E-17	1.72E-17
3	1.13E-15	2.65E-16	2.28E-17	3	9.76E-16	3.54E-16	3.11E-17
4		7.87E-16	3.10E-17	4		8.56E-16	4.88E-17
5			2.77E-17	5			5.05E-17
Σ	1.99E-15	1.26E-15	1.17E-16	Σ	1.61E-15	1.34E-15	1.61E-16
50 keV/u				100 keV/u			
ℓ	n=4	n=5	n=6	ℓ	n=4	n=5	n=6
0	9.89E-18	7.62E-18	5.03E-18	0	9.86E-19	3.66E-19	1.83E-19
1	4.03E-17	2.51E-17	1.66E-17	1	5.50E-18	1.94E-18	1.27E-18
2	1.81E-16	1.16E-16	7.10E-17	2	2.80E-17	8.46E-18	5.04E-18
3	4.07E-16	2.19E-16	1.01E-16	3	1.49E-16	1.84E-17	1.00E-17
4		4.92E-16	1.57E-16	4		1.48E-16	5.57E-17
5			2.01E-16	5			6.91E-17
Σ	6.39E-16	8.59E-16	5.51E-16	Σ	1.83E-16	1.77E-16	1.41E-16
200 keV/u							
ℓ	n=4	n=5	n=6				
0	3.95E-19	2.55E-19	1.98E-19				
1	1.91E-18	1.29E-18	8.97E-19				
2	5.81E-18	4.04E-18	2.72E-18				
3	1.17E-17	7.03E-18	4.86E-18				
4		6.29E-18	5.40E-18				
5			1.26E-18				
Σ	1.99E-17	1.89E-17	1.53E-17				

Table 2: CTMC cross sections for charge transfer in 10, 20, 50, 100, and 200 keV/u Ne^{8+} + H. The table includes the n, ℓ-distribution for n=4, 5, and 6. Cross sections are given in cm^2.

10 keV/u				20 keV/u			
ℓ	n=4	n=5	n=6	ℓ	n=4	n=5	n=6
0	8.06E-17	5.07E-17	1.09E-17	0	5.10E-17	1.69E-17	4.61E-18
1	1.51E-16	1.09E-16	1.82E-17	1	1.27E-16	6.12E-17	1.05E-17
2	2.57E-16	2.36E-16	2.83E-17	2	2.96E-16	2.44E-16	2.47E-17
3	3.97E-16	7.42E-16	5.26E-17	3	4.09E-16	8.02E-16	5.92E-17
4		1.62E-15	8.93E-17	4		1.37E-15	1.14E-16
5			1.23E-16	5			2.17E-16
Σ	8.86E-16	2.76E-15	3.23E-16	Σ	8.84E-16	2.50E-15	4.30E-16
50 keV/u				100 keV/u			
ℓ	n=4	n=5	n=6	ℓ	n=4	n=5	n=6
0	1.55E-17	2.49E-18	1.27E-18	0	2.11E-18	1.89E-18	1.51E-18
1	6.50E-17	1.39E-17	7.73E-18	1	9.80E-18	8.51E-18	6.90E-18
2	2.62E-16	8.77E-17	7.68E-17	2	3.58E-17	2.61E-17	2.04E-17
3	4.29E-16	2.08E-16	1.26E-16	3	8.72E-17	5.26E-17	3.65E-17
4		5.58E-16	1.63E-16	4		1.31E-16	6.71E-17
5			1.34E-16	5			9.90E-17
Σ	7.71E-16	8.70E-16	5.08E-16	Σ	1.35E-16	2.20E-16	2.32E-16
200 keV/u							
ℓ	n=4	n=5	n=6				
0	4.11E-19	2.65E-19	1.77E-19				
1	1.86E-18	1.33E-18	9.71E-19				
2	5.43E-18	3.63E-18	2.81E-18				
3	1.44E-17	7.48E-18	5.27E-18				
4		1.19E-17	7.74E-18				
5			5.06E-18				
Σ	2.21E-17	2.46E-17	2.20E-17				

Table 3: CTMC cross sections for charge transfer in 10, 20, 50, 100, and 200 keV/u Ne^{9+} + H. The table includes the n,ℓ-distribution for n=4, 5, and 6. Cross sections are given in cm^2.

10 keV/u				20 keV/u			
ℓ	n=4	n=5	n=6	ℓ	n=4	n=5	n=6
0	2.48E-17	3.82E-17	1.17E-17	0	2.61E-17	1.84E-17	4.00E-18
1	4.91E-17	1.34E-16	2.59E-17	1	6.59E-17	1.07E-16	1.36E-17
2	7.94E-17	4.02E-16	5.85E-17	2	1.16E-16	4.16E-16	5.60E-17
3	1.06E-16	9.84E-16	1.33E-16	3	1.31E-16	9.32E-16	1.75E-16
4		1.43E-15	3.14E-16	4		1.09E-15	3.35E-16
5			6.69E-16	5			7.47E-16
Σ	2.59E-16	2.99E-15	1.21E-15	Σ	3.40E-16	2.56E-15	1.33E-15
50 keV/u				100 keV/u			
ℓ	n=4	n=5	n=6	ℓ	n=4	n=5	n=6
0	8.81E-18	6.42E-18	1.53E-18	0	4.51E-18	3.14E-18	6.03E-19
1	3.29E-17	2.89E-17	7.67E-18	1	1.62E-17	1.10E-17	4.94E-18
2	9.28E-17	9.88E-17	6.57E-17	2	2.84E-17	2.67E-17	1.14E-17
3	1.71E-16	2.33E-16	1.18E-16	3	3.08E-17	5.70E-17	2.12E-17
4		5.34E-16	2.01E-16	4		1.52E-16	3.87E-17
5			5.25E-16	5			1.75E-16
Σ	3.06E-16	9.02E-16	9.19E-16	Σ	7.99E-17	2.50E-16	2.52E-16
200 keV/u							
ℓ	n=4	n=5	n=6				
0	3.62E-19	2.94E-19	1.96E-19				
1	1.79E-18	1.47E-18	1.18E-18				
2	4.73E-18	3.59E-18	2.79E-18				
3	1.41E-17	7.73E-18	5.56E-18				
4		1.56E-17	9.27E-18				
5			9.24E-18				
Σ	2.10E-17	2.87E-17	2.82E-17				

Table 4: CTMC cross sections for charge transfer in 10, 20, 50, 100, and 200 keV/u Ne^{10+} + H. The table includes the n,ℓ-distribution for n=5, 6, and 7. Cross sections are given in cm^2.

10 keV/u				20 keV/u			
ℓ	n=5	n=6	n=7	ℓ	n=5	n=6	n=7
0	2.47E-17	9.54E-18	3.81E-18	0	1.93E-17	3.69E-18	2.04E-18
1	1.37E-16	4.00E-17	1.08E-17	1	1.29E-16	3.14E-17	7.48E-18
2	3.53E-16	1.30E-16	2.01E-17	2	3.62E-16	1.55E-16	1.51E-17
3	5.56E-16	4.07E-16	3.05E-17	3	5.73E-16	4.32E-16	2.87E-17
4	6.06E-16	9.02E-16	4.89E-17	4	5.27E-16	8.13E-16	5.55E-17
5		1.42E-15	7.55E-17	5		1.17E-15	9.39E-17
6			8.30E-17	6			1.77E-16
Σ	1.68E-15	2.91E-15	2.73E-16	Σ	1.61E-15	2.61E-15	3.80E-16
50 keV/u				100 keV/u			
ℓ	n=5	n=6	n=7	ℓ	n=5	n=6	n=7
0	6.86E-18	6.49E-18	2.89E-18	0	2.00E-18	1.72E-18	1.42E-18
1	4.30E-17	3.78E-17	2.45E-17	1	1.02E-17	8.92E-18	6.64E-18
2	1.30E-16	1.04E-16	6.52E-17	2	2.30E-17	2.00E-17	1.50E-17
3	2.36E-16	1.74E-16	9.40E-17	3	4.85E-17	3.45E-17	2.64E-17
4	2.85E-16	2.97E-16	1.31E-16	4	1.13E-16	6.40E-17	4.32E-17
5		6.26E-16	2.16E-16	5		1.55E-16	7.44E-17
6			4.82E-16	6			1.33E-16
Σ	7.01E-16	1.25E-15	1.02E-15	Σ	1.96E-16	2.84E-16	3.00E-16
200 keV/u							
ℓ	n=5	n=6	n=7				
0	4.07E-19	3.42E-19	2.12E-19				
1	1.41E-18	1.15E-18	1.09E-18				
2	3.38E-18	2.80E-18	2.17E-18				
3	7.28E-18	5.35E-18	3.84E-18				
4	1.82E-17	9.54E-18	7.53E-18				
5		1.51E-17	9.79E-18				
6			7.51E-18				
Σ	3.07E-17	3.42E-17	3.21E-17				

ACKNOWLEDGEMENTS

The authors gratefully acknowledge the support for this work from the US Department of Energy, Office of Fusion Energy, through contract number DE-AC05-84OR21400 with Oak Ridge National Laboratory, managed by Lockheed Martin Energy Systems, Inc.

References

[1] REBUT, P.-H., BOUCHER, D., GAMBIER, D.J., KEEN, B.E., AND WATKINS, M.L., *The ITER Challenge*, 17th Symposium on Fusion Technology, Rome (1992).

[2] POST, D.E., J. Nucl. Mat. **220-222**, 143 (1995).

[3] "Atomic and Molecular Processes in Fusion Edge Plasmas," JANEV, R.K., editor (Plenum Press, New York, 1995).

[4] OLSON, R.E. AND SCHULTZ, D.R., Physica Scripta **T28**, 71 (1989).

[5] SCHULTZ, D.R., MENG, L., REINHOLD, C.O., AND OLSON, R.E., Physica Scripta **T37**, 89 (1991).

[6] ABRINES, R. AND PERCIVAL, I.C., Proc. Phys. Soc. London **88**, 861 (1966).

[7] OLSON, R.E. AND SALOP, A., Phys. Rev. A **16**, 531 (1977).

[8] REINHOLD, C.O., OLSON, R.E., AND FRITSCH, W., Phys. Rev. A **41**, 4837 (1990).

[9] BECKER, R.L. AND MACKELLAR, A.D., J. Phys. B **17**, 3923 (1984).

[10] PEACH, G., WILLIS, S.L., AND MCDOWELL, M.R.C., J. Phys. B **18**, 3921 (1985); WILLIS, S.L., PEACH, G., MCDOWELL, M.R.C., AND BANERJI, J., J. Phys. B **18**, 3939 (1985).

[11] TOBUREN, L.H., DUBOIS, R.D., REINHOLD, C.O., SCHULTZ, D.R., AND OLSON, R.E., Phys. Rev. A **42**, 5338 (1990).

[12] MAYNARD, G., JANEV, R.K., AND KATSONIS K., J. Phys. B **25**, 437 (1992).

[13] LANDAU, L.D. AND LIFSHITZ, E.M., *Quantum Mechanics: Non-Relativistic Theory*, Pergamon, Oxford (1977).

[14] SOLOV'EV, E.A., Zh. Eksp. Teor. Fiz. **81**, 1681 (1981) [Sov.Phys.JETP **54**, 893 (1981)].

[15] SOLOV'EV, E.A., Usp. Fiz. Nauk **157**, 437 (1989) [Sov.Phys.Usp. **32**, 228 (1989)].

[16] OVCHINNIKOV, S.YU. AND SOLOV'EV, E.A., Comments At. Mol. Phys. **22**, 69 (1988).

[17] GROZDANOV, T.P. AND SOLOV'EV, E.A., Phys. Rev. A **42**, 3865 (1990).

[18] KRSTIĆ, P.S. AND JANEV, R.K., Phys. Rev. A **47**, 3894 (1993).

[19] KRSTIĆ, P.S., RADMILOVIĆ, M., AND JANEV, R.K., At. Plasma-Mater. Int. Data Fusion **3**, 113 (1993).

[20] SZYDLIK, P.P. AND GREEN, A.E.S., Phys. Rev. A **9**, 1885 (1974).

[21] FRITSCH, W., in *Review of Fundamental Processes and Applications of Atoms and Ions*, LIN, C.D., editor (World Scientific, Singapore, 1993), p. 239.

[22] SCHULTZ, D.R., KRSTIĆ, P.S., and REINHOLD, C.O., Physica Scripta (1995) to be published.